Hindawi
Mathematical Problems in Engineering
Volume 2021, Article ID 2502476, 13 pages
https://doi.org/10.1155/2021/2502476

*Research Article*

# A Fault Diagnosis Method of Rolling Mill Bearing at Low Frequency and Overload Condition Based on Integration of EEMD and GA-DBN

**Jiang Ji,[1,2] Chen Zhao,[3] Yongqin Wang,[1] Tuanmin Zhao,[2] and Xinyou Zhang[3]**

[1]*Chongqing University, Chongqing 400030, China*
[2]*China National Heavy Machinery Research Institute Co., Ltd, Xi'an 710032, China*
[3]*National Cold Rolling Strip Equipment and Process Engineering Technology Research Center, Yanshan University, Qinhuangdao 066004, China*

Correspondence should be addressed to Xinyou Zhang; 743167051@qq.com

Received 7 June 2021; Accepted 3 November 2021; Published 31 December 2021

Academic Editor: Jaroslaw Latalski



To solve the problems of difficult fault signal recognition and poor diagnosis effect of different damage in the same position in rolling mill bearing at low speed, a fault diagnosis method of rolling mill bearing based on integration of EEMD and DBN was proposed. The vibration signals in horizontal, axial, and vertical directions were decomposed and reconstructed by EEMD, and frequency domain analysis was carried out by using refined spectrum. Then, the signal's time-frequency domain index, rolling force, and torque component feature vector were input into genetic algorithm (GA) to optimize DBN model classification. In order to verify the effectiveness of the method, the experimental study was carried out on the two-high experimental rolling mill. The results show that EEMD combined with thinning spectrum can solve the problem of fault feature extraction well. Compared with time-frequency domain characteristic input, the prediction accuracy of DBN model is obviously improved. And the accuracy of GA-DBN model is higher, and the accuracy is 98.3%, and the time taken to diagnose is significantly reduced. Finally, the fault classification of different parts of bearings and the fault diagnosis of different damage in the same part are realized, which provides a good theoretical basis for the fault diagnosis of low-speed bearings and has important engineering significance.

## 1. Introduction

Rolling bearings are widely used and easily damaged parts in rotary machinery, and their running state directly affects the working performance of the system [1]. The working environment of strip mill is bad. 70% faults of transmission system are related to bearing, and the working state of bearing directly affects the quality of strip products [2]. The development trend of strip rolling mills is high-speed production. Take the 2250 rolling mill of a company as an example; the maximum linear speed of production is 1200 m/min, but the diameter of its work roll is 700 mm, and the maximum rotation speed of the bearing is only 9 r/s. And the speed of finishing mill F1~F4 is only 4.3 r/s, and the speed of bearing in roughing rolling stage is even lower, and its rotation frequency is only 1–3 Hz. Therefore, strip rolling mill bearings are mostly in low-frequency working conditions. In frequency domain analysis, low-frequency features are concentrated on the left end of the spectrum, which is more difficult to identify than high-frequency features, so the frequency analysis of low-frequency bearings is usually more difficult than that of high-frequency bearings. If the low-frequency bearing fault diagnosis can be well realized, it could be applied to high-frequency bearing to achieve better results. In the rolling process, the bearing is subjected to rolling force, so the bearing is in a heavy load state, and the working condition is complex. Therefore, it is urgent to solve the problem of fault feature extraction under low-frequency and heavy load condition of rolling bearing of strip mill and low accuracy of damage diagnosis of different positions.

Extraction of bearing fault feature information from nonlinear and nonstationary vibration signals is the key to

fault diagnosis. In [3], Hu et al. used short-time Fourier transform (STFT) for bearing fault diagnosis, broke through the limitation of traditional time-domain index analysis, and successfully demodulated the periodic component of the modulated signal. In [4], Gao et al. used STFT to process bearing vibration signals and combined with unsupervised nonnegative matrix decomposition to extract fault characteristic frequencies, which proved that the effect of time-frequency domain analysis was significantly better than that of conventional time-domain index analysis. In [5], Wang et al. used the STFT for fault diagnosis of gearboxes and proved that its diagnosis speed is faster than traditional Fourier transform. In [6], Li et al. proposed the interpolation fast Fourier transform of Hamming window. After the signal was processed by Fourier transform, Hamming window was used to carry out the weighted processing, which could realize the accurate identification of bearing fault frequency with fewer analysis points. In [7], Fu et al. used wavelet algorithm to realize rolling bearing fault feature extraction and realize feature extraction of bearing fault impact transient response, which reflected the detection ability of wavelet analysis in processing abrupt signals. In [8], Ai et al. used the peak factor of envelope spectrum to optimize the frequency band of Morlet complex wavelet and applied it to the fault diagnosis of intershaft bearings to realize resonance demodulation processing of vibration signals and extract fault information from vibration signals. In [9], Yang et al. proposed the optimal wavelet scale cyclic spectrum, which well overcame the problem that the results of STFT were greatly affected by the window function, and diagnosed the early weak faults of bearings. In [10], Cheng et al. extracted rolling bearing fault features by chirplet path tracing and realized bearing fault diagnosis under bad working conditions of variable bearing speed and gear noise interference by calculating instantaneous fault feature coefficient, which reflected the excellent noise reduction ability of wavelet analysis.

Although the effect of wavelet analysis has been greatly improved in STFT algorithm, both of them lack adaptability. Therefore, Hung Norden proposed Empirical Mode Decomposition (EMD) [11]. EMD breaks out of the traditional frequency concept and decomposes the signal into multiple modal functions, which has a good adaptive ability. And Wu and Huang proposed the Ensemble Empirical Mode Decomposition (EEMD) algorithm to overcome the shortcomings of EMD by adding uniform white noise [12]. In [13], Cheng et al. used EEMD to extract the feature of rolling bearing vibration signal containing noise, and the frequency domain features were clearer than STFT. In [14], Tian et al. combined EEMD with spatial correlation denoising, the denoising effect of bearing fault signals was better than that of wavelet analysis, and the fault features were more prominent. The above research shows that EEMD algorithm can achieve better results in bearing fault diagnosis compared with STFT, wavelet analysis, and EMD.

Shallow machine learning algorithms have low accuracy when diagnosing complex problems [15]. In order to improve the accuracy of fault diagnosis, scholars combine the fault feature extraction method with deep intelligent algorithm, which greatly improved the accuracy and efficiency of bearing fault diagnosis. In [16], Li et al. combined STFT with convolutional neural network and achieved a high accuracy rate under noise interference. In [17], Liu et al. combined STFT and sparse autoencoder to the bearing fault diagnosis and achieved better results. In [18], Zhao et al. combined wavelet packet with deep belief network (DBN), and the accuracy of fault diagnosis is more than 97%.

Although deep intelligence algorithm can improve the diagnostic accuracy, it needs a large number of samples to train the network, and the training time is long. In [19], Wang et al. directly input EEMD-Hilbert envelope spectrum signals into the DBN and the accuracy of the model is over 95%, but the training time of the model is as long as 6114 seconds, so the identification time problem needs to be solved. In [20, 21], Pan et al. and Yan et al. optimized the structural parameters of neural network by genetic algorithm (GA) and optimized the input of neural network, which greatly improved the speed and accuracy of fault diagnosis. Therefore, this paper uses genetic algorithm to optimize the weight threshold of BP network at the last layer of DBN structure, thus improving the performance and speed of the algorithm. Initial conditions in iterative algorithms can have a large impact on the convergence and stability of the model, so we need to set the initial conditions of the network reasonably to reduce tracking errors in iterative control learning [22, 23]. Therefore, we need to perform feature extraction and noise reduction on the various signals to obtain a better initial input data.

While the above research has only been carried out in the laboratory for the diagnosis of bearing faults, in this paper, we apply the existing mathematical models and algorithms in a real way to the production of real rolling mills. The above studies have done a lot of work on rolling bearing fault diagnosis from the aspects of signal processing and intelligent algorithm, but the particularity of rolling mill structure and working environment has not been considered. The lack of fault data in the actual production process of the factory, the insufficient training of the initial model of the fault diagnosis system, and the fact that diagnosis still depends on frequency domain analysis have not been taken into account. And fault diagnosis of low-speed and heavy-duty bearings has not been carried out. In this paper, rolling mill bearing vibration signals are processed by EEMD to solve the problems of large vibration signal interference and noise, long fault impulse response period, and low fault characteristic frequency, which are difficult to extract. Then, analyze the signal by zoom spectrum and extract the fault features. Aiming at the problem that it is difficult to accurately identify the fault position and damage degree of rolling mill bearing due to the changes of metal size and rolling force during rolling process, BP network optimization was optimized by genetic algorithm as the last layer of DBN to realize fault diagnosis and identification. Finally, the method of rolling mill bearing fault diagnosis based on EEMD and DBN is formed, and the fault diagnosis of different damage in the same part of rolling mill bearing is realized.

## 2. Mathematical Model

*2.1. EEMD Algorithm.* EEMD is an improvement of EMD. After the signal is decomposed by EEMD, the last component is removed, and the signal is reconstructed, which can improve the signal-to-noise ratio of the signal. Literature 14 shows that the frequency domain characteristics of rolling bearing signals processed by EEMD are more obvious. In [24], Kong et al. successfully separated double bearing impact features by using EEMD to process the signal. Therefore, EEMD can effectively solve the problems of bad working environment of rolling mill and large signal noise interference, and a better effect can be achieved in noise reduction processing of vibration signals.

EMD is an adaptive analysis method, which breaks away from the definition of frequency in Fourier transform and introduces the concept of instantaneous frequency. And EMD can achieve good results in nonstationary and nonlinear signal processing. The algorithm decomposes the signal into multiple IMF components, and each IMF component contains local characteristic signals at different time scales. The specific steps are as follows:

(1) The original signal $x(t)$ is subtracted from the mean envelope $m(t)$ to obtain the signal $h(t)$, denoted as IMF1.

$$h(t) = x(t) - m(t). \tag{1}$$

(2) The first IMF component is removed from the original signal $x(t)$, and the residual $r(t)$ can be obtained:

$$r(t) = x(t) - \text{IMF1}. \tag{2}$$

(3) The residual $r(t)$ is brought back to the first step to obtain IMF2 and IMF3, and the last residual $r(t)$ is EMD residual component and satisfies the following relation:

$$x(t) = \sum \text{IMF} + r(t). \tag{3}$$

EEMD needs to add white noise $w_i(t)$ with total mean zero to the original signal, and the original signal $x(t)$ becomes $y_i(t) = x(t) + w_i(t)$. The new signal is decomposed by EMD, and J IMF components and residual components are obtained as follows:

$$y_i(t) = \sum_{j=1}^{J} c_{ij} + r_i. \tag{4}$$

Repeat the above steps and get an average of IMF$d_j$ for the components as follows:

$$d_j = \frac{1}{I} \sum_{i=1}^{I} c_{ij}. \tag{5}$$

*2.2. ZOOMFFT Refine Spectrum.* In order to preliminary realize the fault diagnosis, the signal needs to be analyzed in the frequency domain. Compared with cepstrum and energy spectrum, envelope spectrum can achieve better results in the processing of early fault signals. However, the characteristic frequencies of low-frequency and heavy-load bearing fault signals are concentrated at the left end of the spectrum, and the frequency is less than 10 Hz. The amplification of envelope spectrum will cause the spectrum resolution to decrease, and the processing effect will be worse. Zoom spectrum can improve the resolution of the spectrum, realize the amplification of the frequency region, and get more accurate spectrum amplitude, phase, and frequency. In [25, 26], Xia et al. successfully solved the problem that the low resolution of Teager energy operator and Hilbert transform could not demodulate low-frequency modulation signal by using zoom spectrum. Therefore, zoom spectrum is better than envelope spectrum in the frequency domain analysis of low-frequency fault vibration signals.

Therefore, the spectrum of rolling mill bearing needs to be refined by zoom spectrum. In this paper, we use ZoomFFT to refine the spectrum of rolling mill bearing signals. FFT can only analyze the signal from the zero frequency, but ZoomFFT can greatly refine the spectrum, ZoomFFT can move the narrowband spectrum to near the zero frequency, and then the signal is processed by FFT.

Signal $x(t)$ is processed by A/D sampling, and a discrete signal sequence $x(n)$ is obtained. The sampling frequency is $f_s$, the center frequencies of the refining frequency band are $f_1$ and $f_2$, the center frequency is $f_e$, the number of points selected is $N$, and the specific process is as follows:

(1) Discrete FFT of the processed signal is

$$X_0(k) = \sum_{n=0}^{N-1} x_0(n) W_N^{mk} \quad (k = 0, 1, \ldots, N-1), \tag{6}$$

$$W_N = e^{-j2\pi/N}. \tag{7}$$

The processed signal is complexly modulated with the frequency band center frequency $f_e = (f_1 + f_2)/2$, and the frequency shift signal is obtained as

$$x(n) = x_0(n) e^{-j2\pi n f_e / N f_s}, \tag{8}$$

$$x(n) = x_0(n) \cos \frac{2\pi n L_0}{N} - j x_0(n) \sin \frac{2\pi n L_0}{N}, \tag{9}$$

where the sampling frequency is $f_s = N \times f$, interval of spectral line is Df, and the displacement of frequency center is $L_0 = f_e/f$.

According to the frequency shift property of Fourier transform, the relation between the discrete spectrum $X(k)$ of the signal and the discrete spectrum $X_0(k)$ of $x_0(n)$ is

$$X(k) = X_0(k + L_0). \tag{10}$$

(2) Set the refining multiple $D$ and the cut-off frequency of the low-pass filter is $f_e = f_s/2D$, and the filter output is

$$y(n) = \frac{1}{N}\sum_{k=0}^{N-1} X(k)H(k)W_N^{-nk}, \tag{11}$$

where the frequency response of the low-pass filter is $H(k)$.

(3) Resampling with frequency $f_s' = f_s/D$ is adopted to obtain the time-domain signal $g(m) = y(m)$, which is obtained by equations (6)–(10):

$$g(m) = \frac{1}{N}\left\| \sum_{P=0}^{N/2-1} X_0(p + L_0)W^{-pm} + \sum_{p=N/2}^{N-1} (p - N + L_0)W^{-pm} \right\|. \tag{12}$$

(4) Finally, perform the FFT again and adjust the frequency to complete the ZoomFFT. The flow chart of ZoomFFT is shown in Figure 1:

*2.3. Genetic Algorithm Optimization of DBN.* DBN is composed of restricted Boltzmann machine (RBM) and a reverse fine-tuning BP network. In order to solve the problem that the last layer BP network of DBN is prone to fall into local minimum value and run slowly during training, we adopt genetic algorithm to optimize BP network. The layer structure parameters of the DBN in this paper are shown in the following Table 1. The network structure is shown in Figure 2.

(1) Determine the topology structure of the neural network, and determine the number of input layer $R$, hidden layer $S_1$ and output layer $S_2$ and the code length $S$. The formula is shown as follows:

$$S = R \times S_1 + S_1 \times S_2 + S_2. \tag{13}$$

(2) Establish the last layer of BP network, and use the corresponding dimensional variable to represent the number of network weight thresholds. The gene formula after coding is shown as follows:

$$X = \left[\omega_{11}...\omega_{nm}, \nu_{11} \ldots \nu_{pm}, \theta_1 \ldots \theta_m, t_1 \ldots t_p\right], \tag{14}$$

where $v_{ij}$ is the threshold of the $j$-th neuron of the input layer to the $i$-th neuron of the hidden layer, $n_{ij}$ is the threshold of the $j$-th neuron of the hidden layer to the $i$-th neuron of the output layer, $u_i$ is the threshold of the $i$-th neuron in the hidden layer, and $t_i$ is the threshold of the $i$-th neuron in the output layer.

(3) Use training and test samples to train and test the network separately, calculate the sum of squared test errors SE, and take the reciprocal of SE as the fitness value of the genetic algorithm:

$$\mathrm{Val} = \frac{1}{\mathrm{SE}}. \tag{15}$$

(4) The excellent individuals are selected in the form of roulette wheel, and the excellent individuals of the previous generation are single-point crossed to enlarge a certain coding value of the individuals of the population, so as to improve the random search ability of the algorithm.

(5) The optimization process of (3) and (4) is repeated continuously until the termination conditions are met and the optimal neural network weights and thresholds are obtained. The optimization of DBN by genetic algorithm is completed.

The optimized process is shown in Figure 3.

*2.4. Rolling Mill Bearing Fault Diagnose Method Based on EEMD and DBN.* EEMD and zoom spectrum can effectively solve the problem of high noise of rolling mill bearing vibration signal and difficulty in extracting fault characteristic frequency. Bearing faults can be preliminarily diagnosed according to the fault characteristic frequency, but intelligent identification of bearing faults cannot be realized, and the diagnosis results depend on experience. DBN has excellent classification and prediction ability, but the strong ability of DBN depends on sufficient training samples and good input vector. In this paper, we combine EEMD with DBN. First, EEMD is used to process the vibration signal to preliminary identify the fault. Next, extract the feature vector as the input of the DBN and train the network. Finally, classify the feature vectors by DBN network. EEMD and DBN complement each other, EEMD solves the input problem of DBN, as well as the problem of insufficient training samples in the early stage of diagnosis and low diagnostic accuracy, and DBN solves the problem that EEMD cannot intelligently realize fault identification. Finally, a fault diagnosis model of EEMD and GA-DBN is established, and the fault diagnosis process is shown in Figure 4. The effective combination of the two algorithms can improve the accuracy and efficiency of rolling mill bearing fault diagnosis and finally realize the fault diagnosis of rolling mill bearing with different damage degrees.

## 3. The Experiment of Rolling Mill Bearing Fault Diagnose

The equipment used in this test mainly includes experimental rolling mill, sensor, and data acquisition equipment. The test bench is shown in Figure 5. The parameters of the rolling mill are as follows: the diameter of roll is 120 mm, the length of roll is 90 mm, the rotation of main motor is 18 r/min, the maximum rolling force is 12 tons, the vibration sensor is YS8202 acceleration sensor, the pressure sensor model is HZC-01 to measure the rolling force, and the torque sensor model is BHF350 to measure the torque of the transmission shaft.

The work roll bearing of the experimental rolling mill is a single row cylindrical roller bearing installed side by side, and its model is NU1012. The vibration signals of 8 sets of normal bearings, 2 sets of rolling body wear group bearings, 2 sets of cage damage group bearings, and 2 sets of rolling

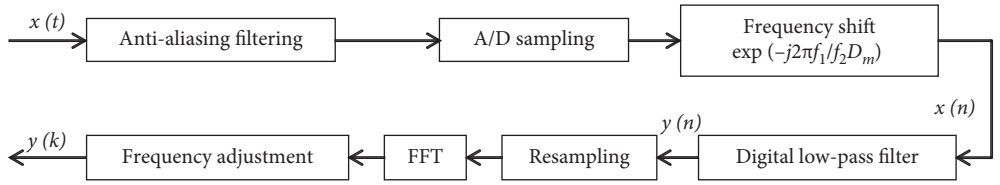


Figure 1: The flow chart of ZoomFFT.

Table 1: The layer structure parameters of the DBN.

| Layer | Number of neurons | Learning rate |
|---|---|---|
| Input | 127 | 0.01 |
| First hidden layer | 127 | 0.01 |
| Second hidden layer | 10 | 0.01 |
| Third hidden layer | 10 | 0.01 |
| Output | 1 | 0.01 |

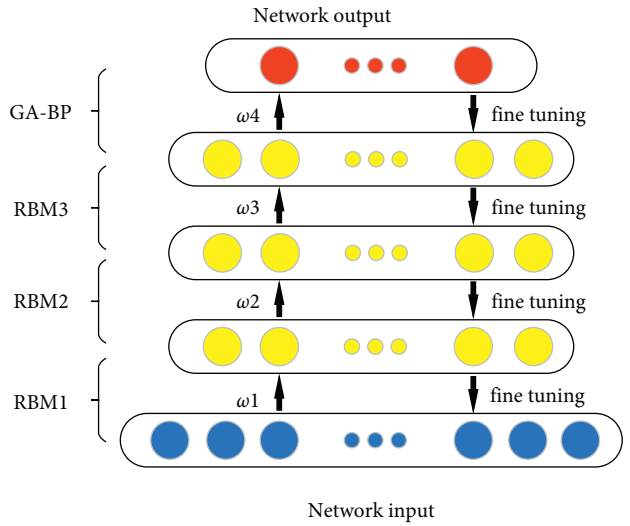


Figure 2: The structure of optimization DBN using GA.

body spalling group bearings were collected with the test bench and the equipment mentioned above.

The working conditions of the roll are set as 5.04 r/min and 3.96 r/min, and the reduction amount is 25% and 40%. Then, collect the vibration signals of the above four groups of bearings along $X$, $Y$ and $Z$ axes, rolling force signals of the rolling mill driving side and operating side, and torque signals of the upper and lower drive shafts. And the sampling frequency is 2000 Hz.

The signal time domain diagram with the speed of 5.04 r/min and the reduction of 40% is shown in Figure 6. The first 2 seconds of the rolling mill is in the no-load state, and the signal amplitude is small. After the 51st second, due to steel throwing phenomenon, the amplitude increased sharply. Therefore, the signals at both ends are discarded, and the stationary signal in the middle is taken as the frequency domain diagram as shown in Figure 7:

The rolling bearing of the rolling mill has a low rotation speed and a low fault characteristic frequency, which is concentrated on the left side of the spectrum diagram, and effective information cannot be obtained from the frequency domain diagram shown. Therefore, it is necessary to process vibration signal and extract the fault features by EEMD and zoom spectrum. By this method, we could extract the bearing fault characteristic frequency and accurately identify the bearing fault.

## 4. Results and Discussion

*4.1. Calculation of Fault Characteristic Frequency.* The fault characteristic frequency of each component of the bearing is shown in Table 2:

*4.2. Results of EEMD and ZOOM Spectrum.* Several components of vibration signals obtained after EEMD processing (showing the first 5 components with high correlation with the original signal) are shown in Figure 8. IMF1 still has more noise energy, while IMF2 and IMF3 have impact characteristics.

The correlation coefficient provides a good response to the correlation between the component signals and the original signal, so we use it as a criterion for judging the IMF. Calculate the correlation coefficient between the original signal and each IMF component; the correlation coefficient of IMF1, IMF2, and IMF3 is 0.6292, 0.2309, and 0.0452. Because the correlation coefficient between the components after IMF4 and the original signal is very low, little fault information is included, so the components after IMF4 are discarded. And take the first three components for signal reconstruction, and then the reconstructed signal is processed by zoom spectrum to realize the preliminary diagnosis.

The analysis spectrum diagram of rolling body fault signal with a rotating speed of 5.04 r/min is shown in Figure 9. The frequency display range is 0~2.5 Hz, the theoretical rotation frequency is 0.084 Hz, and the rolling body fault frequency is 0.36 Hz. As shown in the figure, the maximum peak frequency 0.08125 Hz is the rotation frequency, and the peak frequency 0.1667 Hz is the double rotation frequency. The frequency peak of 0.3542 Hz is the rolling body fault frequency peak, and the frequency peaks of 0.7875 Hz and 1.106 Hz are the double and triple rotation frequency of the rolling body fault frequency, respectively. Compared with the envelope spectrum of the same signal as shown in Figure 10, it can be seen that the resolution of the signal processed by the envelope spectrum is obviously insufficient, and the characteristic frequency peak may not be displayed due to the low resolution. The processing effect of the envelope spectrum is worse than that of the zoom spectrum, and the fault characteristic frequency cannot be recognized normally.

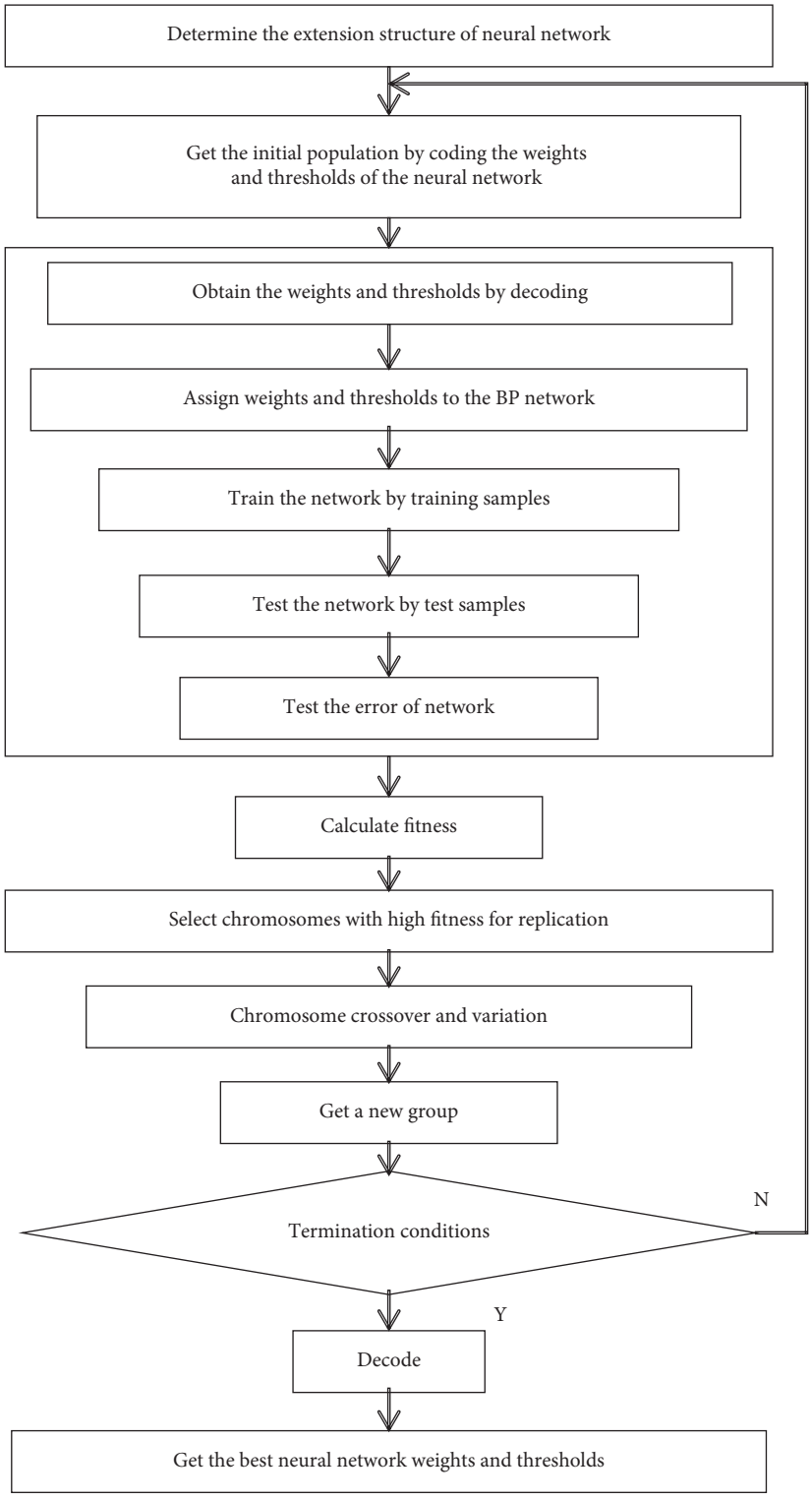


Figure 3: The flow chart of the optimization BP using GA.

The analysis spectrum diagram of normal bearing signal with a rotating speed of 3.96 r/min is shown in Figure 11. The frequency display range is 0~2.5 Hz, and the theoretical rotation frequency is 0.066 Hz.

As shown in the figure, the maximum peak frequency 0.0625 Hz is the rotation frequency, and the frequency peaks of 0.1042 Hz and 0.2083 Hz are the double and triple rotation frequency of rotation frequency, respectively.

Compared with Figure 8, the spectrum in Figures 9 and 11 is clearer. EEMD and zoom spectrum can realize the extraction of the fault characteristic frequency of rolling bearings with low rotating speed. And the effective

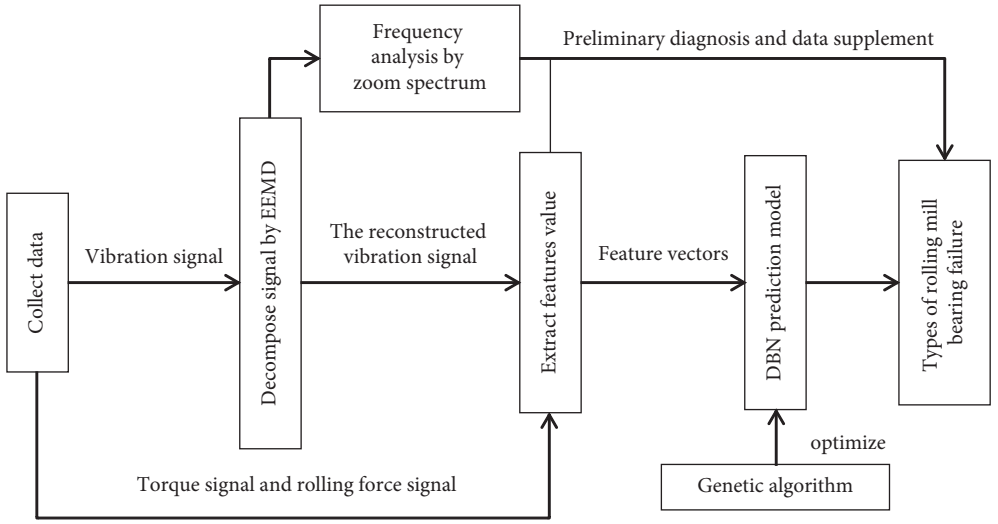


Figure 4: The flow chart of bearing fault diagnosis.

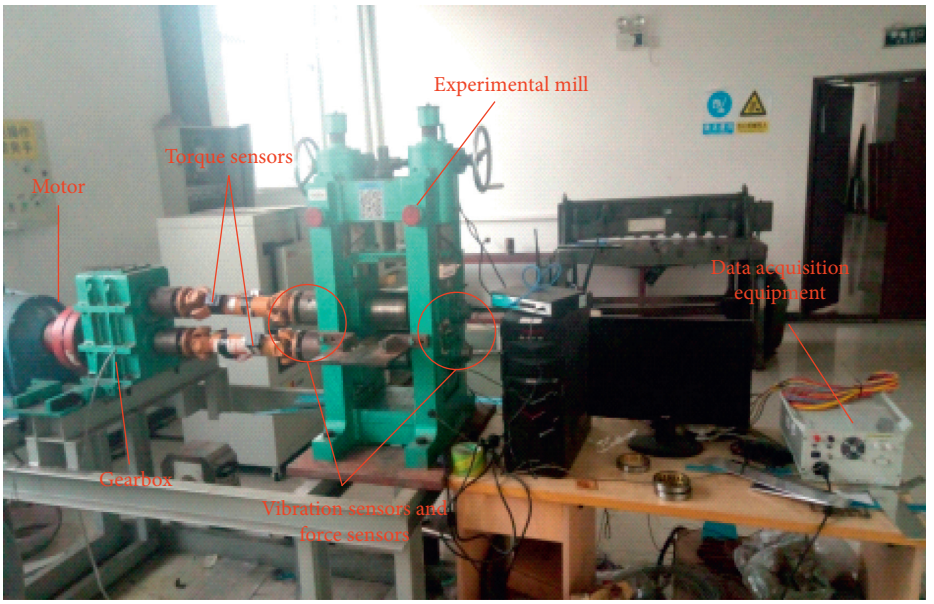


Figure 5: The rolling mill experiment platform.

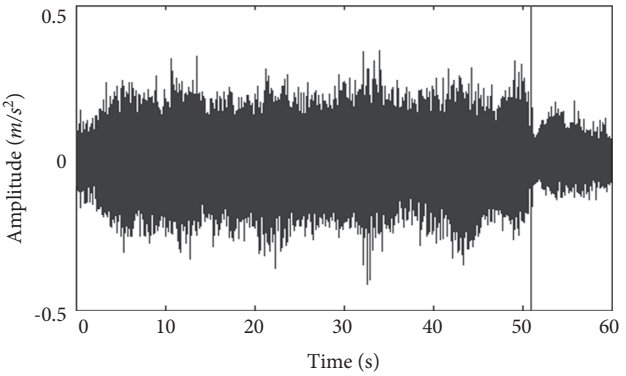


Figure 6: Time domain diagram of speed 5.04 r/min signal.

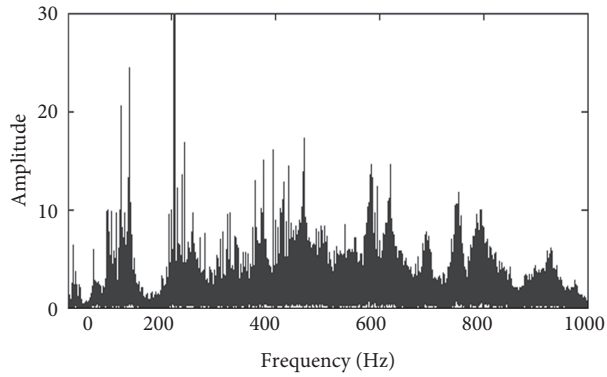


Figure 7: Frequency domain diagram of stable signal.

Table 2: Characteristic frequency of bearing fault.

| Fault types | The 5.04 r/min group | The 3.96 r/min group |
|---|---|---|
| Inner ring fault (Hz) | 1.065 | 0.839 |
| Outer ring fault (Hz) | 0.862 | 0.673 |
| Roller fault (Hz) | 0.388 | 0.306 |
| Cage failure (Hz) | 0.037 | 0.029 |

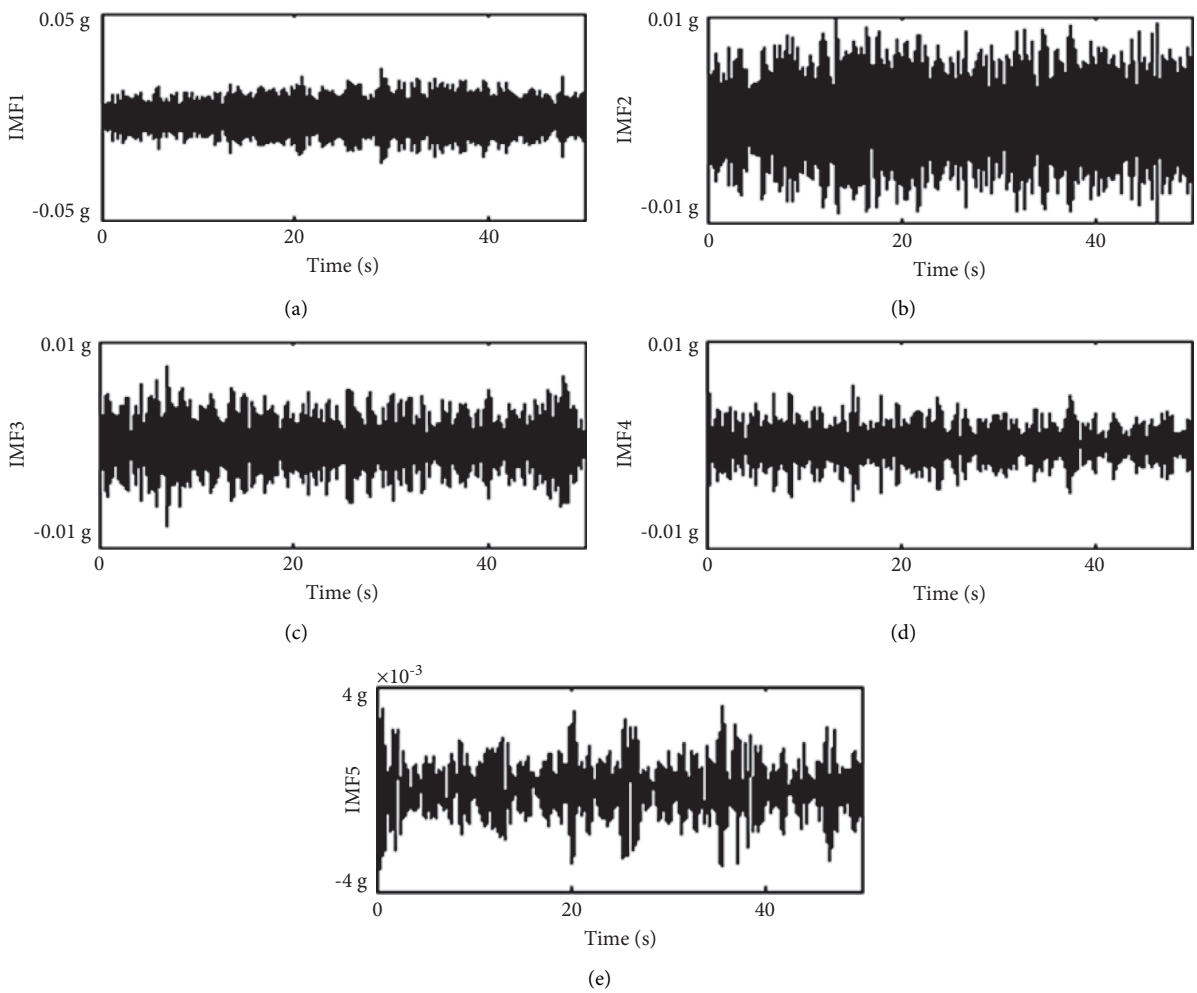


Figure 8: Time domain diagram of IMF. (a) IMF1, (b) IMF2, (c) IMF3, (d) IMF4, and (e) IMF5.

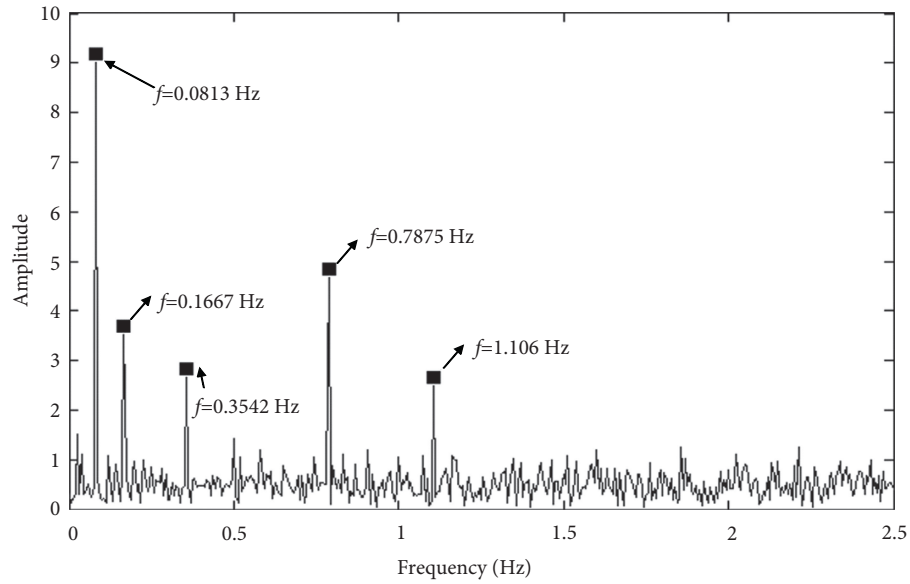


Figure 9: Refinement spectrum of rolling body fault bearing with rolling speed of 5.04 r/min.

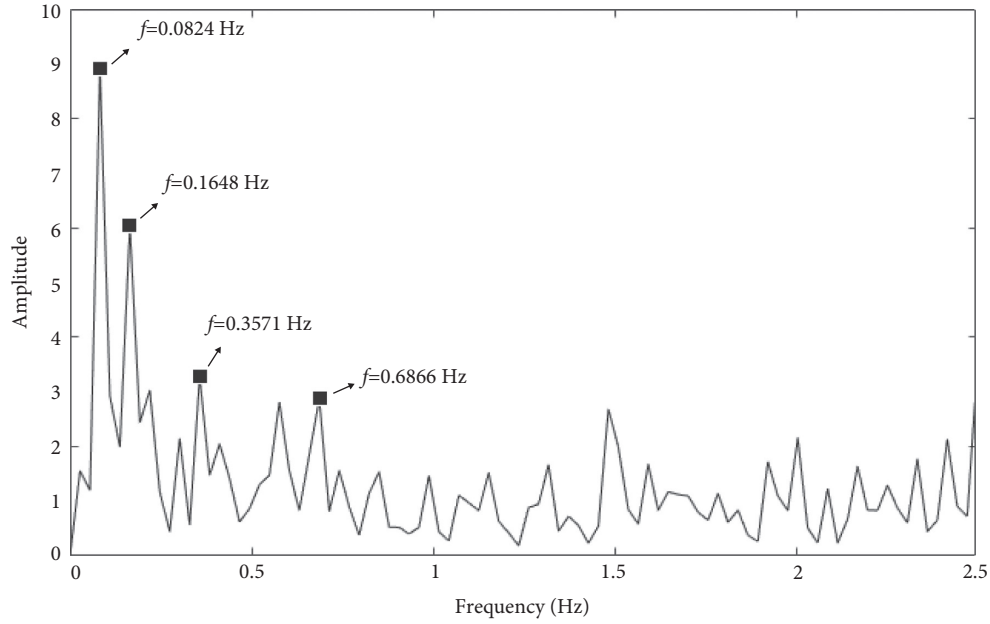


Figure 10: Envelope spectrum of rolling body fault bearing with rolling speed of 5.04 r/min.

combination of the two methods can realize the determination of the fault location of rolling mills bearings.

*4.3. Comparative Analysis of GA-DBN and DBN Classification Results.* The first three IMF components are used to calculate nine time-domain indicators (including maximum value, minimum value, average value, standard deviation, root mean square value, skewness value, peak-to-peak value, kurtosis value, and waveform factor) and two frequency indicators (including the center frequency and frequency variance). And the rolling force signals of the driving side and the operating side as well as the torque signals of the upper shaft and the lower shaft are used to calculate seven time-domain indicators (including the maximum value, minimum value, average value, standard deviation, skewness value, peak-to-peak value, and kurtosis value).

The initial conditions in iterative algorithms can have a large impact on the convergence and stability of the model, so we need to set the initial conditions of the network reasonably to reduce tracking errors in iterative control learning [22, 23]. Therefore, it is necessary to process the data reasonably and to design the initial conditions of the network structure reasonably. The eigenvector of [S1, S2, S3, N1, N2, F1, F2] is composed of the characteristic values of vibration signals, torque signals, and rolling force signals of

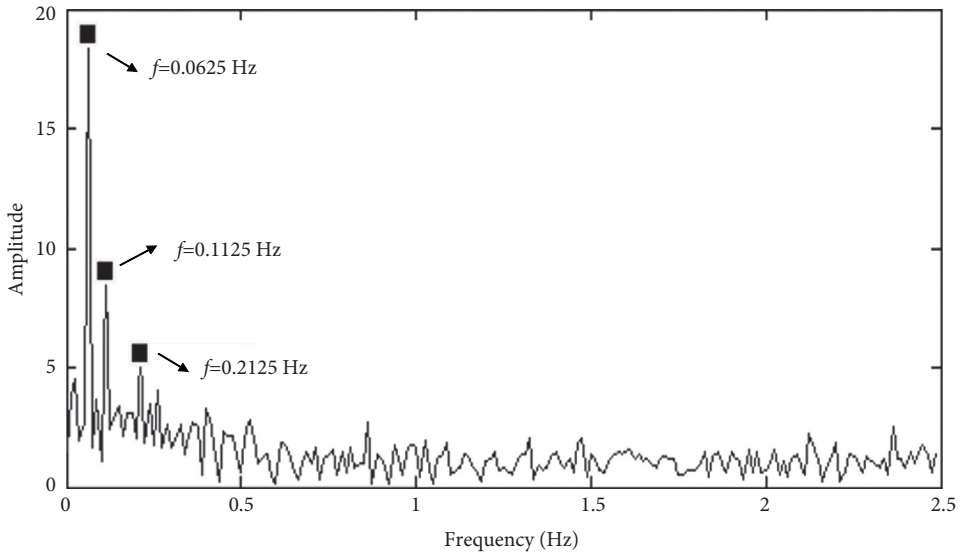


Figure 11: Refinement spectrum of normal bearing with speed of 3.96 r/min.

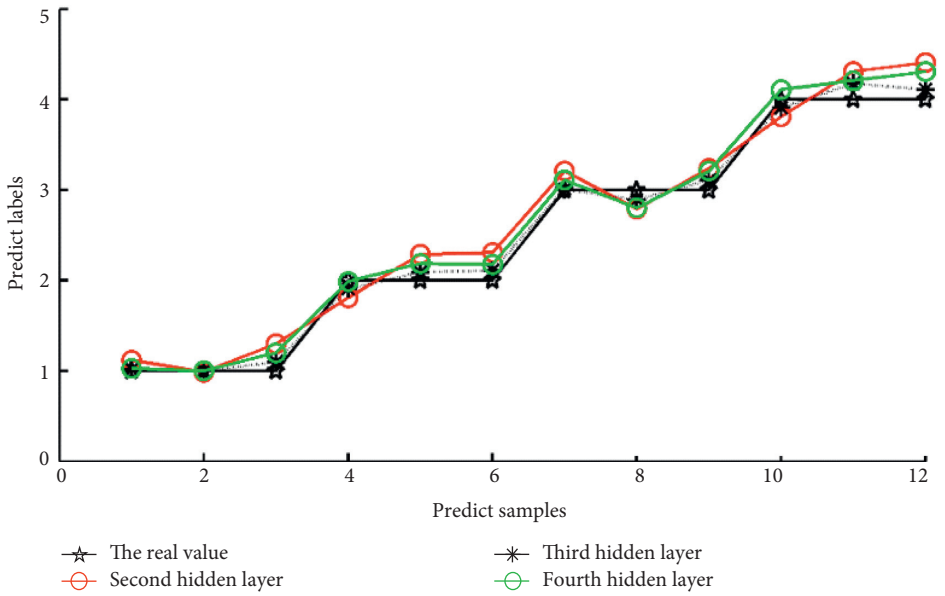


Figure 12: The forecast chart using GA-DBN algorithm.

various faults. The dimension of S1~S3 is 11, representing 9 time-domain indicators and 2 frequency-domain indicators of vibration signals in three directions of the bearing seat, respectively. The dimensions of N1 and N2 are 7, representing 7 time-domain indicators of upper and lower shaft torque signals, respectively. The dimensions of F1 and F2 are 7, representing 7 time-domain indicators of rolling force signals of rolling mill operation measurement and transmission side. Feature vector with dimension 127 is used to represent the characteristic information of various fault vibration signals as the input vector for DBN.

The labels of normal bearings are set to 1, the labels of cage damage bearings are set to 2, the labels of roller surface wear bearings are set to 3, and the labels of roller surface peel bearings are set to 4.

The eigenvectors are put into the GA-DBN and the ordinary DBN for training, and predict the eigenvalues of the second, third, and fourth hidden layers. The results are shown in Figures 12 and 13:

The root-mean-square error of the hidden layer of the network can well characterize the specific performance of the network, so we use it as a performance evaluation index and guide the setting of the network structure. The root-mean-square errors of each hidden layer of DBN optimized by genetic algorithm are 0.0730, 0.0283, and 0.0499, and the root-mean-square errors of each hidden layer of

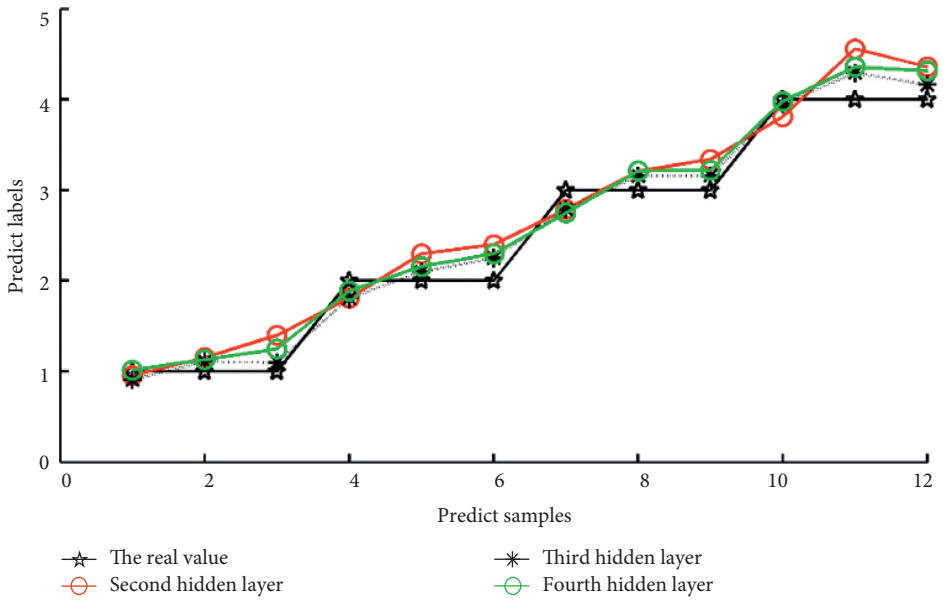


Figure 13: The forecast chart using DBN algorithm.

Table 3: The performance parameters of the model.

| Structure | Model | The root-mean-square errors |
|---|---|---|
| Two hidden layers | DBN | 0.0730 |
| Three hidden layers | DBN | 0.0283 |
| Four hidden layers | DBN | 0.0499 |
| Two hidden layers | GA-DBN | 0.0897 |
| Three hidden layers | GA-DBN | 0.0493 |
| Four hidden layers | GA-DBN | 0.0641 |

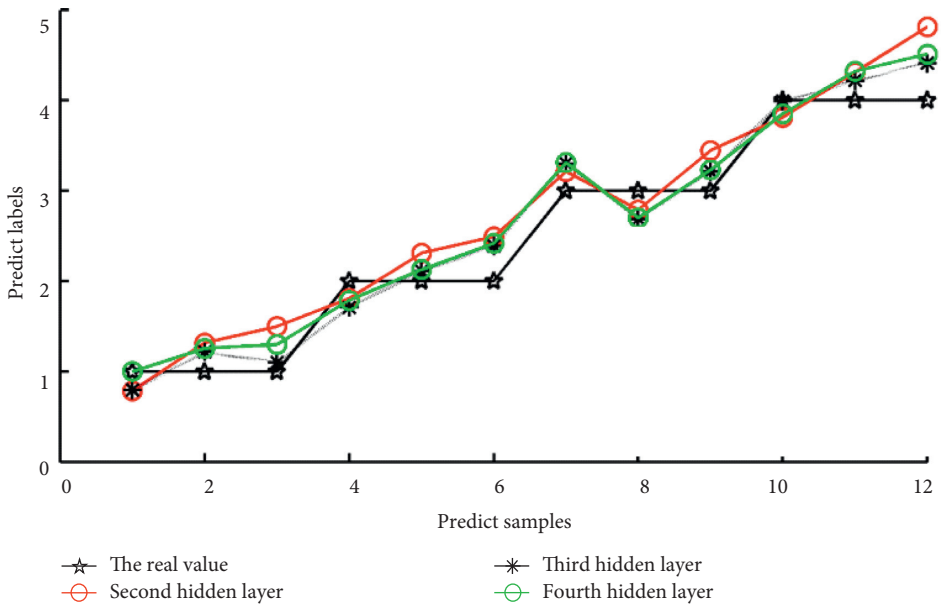


Figure 14: GA-DBN prediction chart without roll force and torque.

Table 4: Comparison of models for various input conditions.

| Input | Model | Best accuracy (%) | Time (s) |
|---|---|---|---|
| Time domain signals | DBN | 85.6 | 5427 |
| Time domain features of vibration signals | DBN | 82.1 | 321 |
| Time domain features of all signals | DBN | 92.5 | 403 |
| Time domain signals | GA-DBN | 87.3 | 5803 |
| Time domain features of vibration signals | GA-DBN | 85.0 | 357 |
| Time domain features of all signals | GA-DBN | 98.3 | 431 |

conventional DBN are 0.0897, 0.0493, and 0.0641. The performance parameters of the model obtained under different hidden layer conditions are shown in Table 3.

Because the root-mean-square error of the third hidden layer is the smallest, the optimal hidden layer number of DBN is determined to be 3. And the prediction results of each hidden layer of GA-DBN are better than the conventional DBN, because the genetic algorithm can jump out of the local minimum point through crossover and mutation, which overcomes the shortcomings of BP network.

A total of 120 test samples were randomly selected to test the accuracy of the prediction model. The prediction accuracy of GA-DBN model with three hidden layers was 92.5%, 98.3%, and 97.5%, respectively, while that of the conventional DBN model was 87.5%, 94.2%, and 92.5%, respectively. It can be concluded that when the number of hidden layers is three optimal layers, the accuracy of GA-DBN algorithm was the highest, and the accuracy is 98.3%. And the accuracy of each hidden layer of GA-DBN algorithm is higher than that of conventional DBN algorithm. It can be confirmed that the prediction accuracy of GA-DBN proposed in this paper has been improved compared with that of conventional DBN.

*4.4. Comparative Analysis of NON-LOAD Input Network Model.* The prediction graph of GA-DBN without rolling force and torque signal input is shown in Figure 14. Compared with Figure 11, the simulation results prove that the identification accuracy of network with rolling force and torque signal input is higher.

The accuracy of the model without rolling force and torque input is 77.5%, 88.3%, and 85.0%, and the highest prediction accuracy of the model is 88.3%, which is 10 percentage points lower than that of the mixed input model 98.3%, thus proving the effectiveness of the mixed prediction model.

The final results show that the training time of the force and torque input model and the strength and torque input model is 431 s and 357 s, respectively. Compared with the training time of 6114 s when Wang et al. [19] directly used spectral signal as input model, the training time was greatly shortened. And the results can prove that the method proposed in this paper can effectively shorten model training time. And the results of the model comparison under various input conditions are obtained as shown in Table 4.

## 5. Conclusions

This paper differs from existing laboratory research by applying mathematical models and networks to actual rolling production, enabling condition monitoring and fault diagnosis of mill bearings.

(1) It is difficult to extract fault features from bearing signals of strip rolling mill under low frequency and heavy load condition, and the diagnosis effect of bearing with different damage at the same position is poor. In order to solve this problem, EEMD is used to realize fault feature extraction, and GA-DBN is used for fault diagnosis. Finally, the fault diagnosis model of heavy-duty bearing is established.

(2) By analyzing the vibration data of the experimental rolling mill, the results show that the signal reconstruction by EEMD can effectively realize the signal noise reduction. We could accurately extract the characteristic frequency and preliminarily diagnose faults of low-frequency bearing faults by zoom spectrum. It is proved that the GA-DBN model has high accuracy in fault feature recognition.

(3) The experimental results show that the prediction accuracy of GA-DBN model is significantly improved by 10 percentage points by adding rolling force and torque signals as feature vectors, which proves the advantages of the method in this paper.

In this paper, we have achieved fault diagnosis of rolling mill bearings. However, the amount of data from vibration signals in signal processing still has a large impact on model calculations, and we still need to work in the direction of data processing in the future. And our model is built under steady state conditions and does not take into account the difficulty of obtaining data, so in future work, we need to further develop fault diagnosis under small samples and variable conditions, and the application of GAN [27] provides a good solution to the above problem, which will be our future work.

## Data Availability

The experimental data can be obtained through request (743167051@qq.com). The experimental data were obtained through the rolling experiment of National Cold Rolling Strip Equipment and Process Engineering Technology Research Center of Yanshan University. The experimental results are reproducible. Relevant scholars can use similar experimental models or go to the National Cold Rolling Strip Equipment and Process Engineering Technology Research Center of Yanshan University to further verify the reliability of the experimental data.

## Conflicts of Interest

The authors declare that they have no conflicts of interest.

## Authors' Contributions

Z. X. Y., J. J,. and Z. C. conceived the initial idea; Z. C and Z. X. Y. wrote the article. Z. X. Y. conducted experiments to collect data; J. J., Z. C., and Z. Y. X. analyzed the data; W. Y. Q. and Z. T. M. provided experimental equipment and fund.

## Acknowledgments

This research was supported by 2018 National Machinery Group Major Science And Technology Project "development and application of high quality wide aluminum alloy plate and strip efficient cold rolling mill" (Grant no. SINOMAST-ZDZX-2018-06) and Central Government's Funding for Local Science and Technology Development (Grant no. 216Z1802G).

## References

[1] M. Zhang, Z. Y. Cai, and S. Bao, "Fault diagnosis of rolling bearing based on EEMD-Hilbert and FWA-SVM," *Journal of Southwest Jiaotong University*, vol. 54, no. 3, pp. 633–639,662, 2019.

[2] F. Liu, *Study on Intelligent Fault Diagnosis System of the Cold Rolling Mill*, Dong Ben University, Da Nang City, Vietnam, 2013.

[3] X. Y. Hu, Q. F. He, and H. S. Wang, "Vibration signal demodulation method based on STFR and ITS application in rolling bearing fault detections," *Journal of Vibration and Shock*, no. 2, pp. 82–86,178, 2008.

[4] H. Z. Gao, L. Liang, X. G. Chen, and G. Xu, "Feature extraction and recognition for rolling element bearing fault utilizing short-time fourier transform and non-negative matrix factorization," *Chinese Journal of Mechanical Engineering*, vol. 28, no. 1, 2015.

[5] Y. R. Wang, J. Wang, and H. A. Huang, "Fault diagnosis of planetary gearbox based on NLSTFT order tracking under variable speed conditions," *China Mechanical Engineering*, vol. 29, no. 14, pp. 1688–1695, 2018.

[6] X. Y. Li, Z. J. Xie, and J. F. Luo, "Applications of windowed interpolation FFT algorithm in rolling bearing fault diagnosis," *China Mechanical Engineering*, vol. 29, no. 10, pp. 1166–1172, 2018.

[7] Q. Fu, Y. C. Zhang, L. J. Ying, and G. Li, "Extraction of failure character signal of rolling element bearings by wavelet," *Chinese Journal of Mechanical Engineering*, vol. 37, no. 2, pp. 30–32, 37, 2001.

[8] T. Ai, B. W. Tian, and J. Tian, "Frequency band optimization of morlet complex wavelet and its application in fault diagnosis of inter-shaft bearing," *Journal of Aerospace Power*, vol. 35, no. 1, pp. 153–161, 2020.

[9] R. Yang, H. K. Li, and C. B. He, "Rolling element bearing incipient fault feature extraction based on optimal wavelet scales cyclic spectrum," *Journal of Mechanical Engineering*, vol. 54, no. 17, pp. 208–217, 2018.

[10] W. D. Cheng, D. Liu, and D. Z. Zhao, "fault feature extraction method for rolling bearings based on chirplet path tracing," *Journal of Vibration and Shock*, vol. 36, no. 13, pp. 155–160, 200, 2017.

[11] E. Hung Norden, S. Zheng, R. Long Steven et al., "The empirical mode decomposition and the Hilbert spectrum for nonlinear and non-stationary time series analysis," *Proceedings of the Royal Society A: Mathematical, Physical & Engineering Sciences*, vol. 454, no. 1971, pp. 743–761, 1998.

[12] Z. Wu and N. E. Huang, "Ensemble empirical mode decomposition: a noise-assisted data analysis method," *Advances in Adaptive Data Analysis*, vol. 1, no. 1, pp. 1–41, 2009.

[13] J. S. Cheng, J. Wang, and L. Gui, "An improved EEMD method and its application in rolling bearing fault diagnosis," *Journal of Vibration and Shock*, vol. 37, no. 16, pp. 51–56, 2018.

[14] J. Tian, Y. J. Wang, Z. Wang, and Y. Ai, "Fault diagnosis for rolling bearing based on EEMD and spatial correlation denoising," *Chinese Journal of Scientific Instrument*, vol. 39, no. 7, pp. 144–151, 2018.

[15] Y. N. Zhang, W. Wei, and L. Wu, "Motor mechanical fault diagnosis based on wavelet packet, Shannon entropy, SVM and GA," *Electric Power Automation Equipment*, vol. 30, no. 1, pp. 87–91, 2010.

[16] H. Li, Q. Zhang, X. R. Qin, and Y. Sun, "fault diagnosis method for rolling bearings based on short-time fourier transform and convolution neural network," *Journal of Vibration and Shock*, vol. 37, no. 19, pp. 124–131, 2018.

[17] H. M. Liu, L. F. Li, and J. Ma, "Rolling bearing fault diagnosis based on STFT-deep learning and sound signals," *Shock and Vibration*, vol. 2016, Article ID 6127479, 12 pages, 2016.

[18] G. Q. Zhao, Z. D. Jiang, and C. Hu, "Bearing fault diagnosis based on wavelet packet energy entropy and DBN," *Journal of Electronic Measurement and Instrument*, vol. 33, no. 2, pp. 32–38, 2019.

[19] Y. J. Wang, X. D. Na, S. Q. Kang, and J. Xie, "State recognition method of a rolling bearing based on EEMD-Hilbert envelope spectrum and DBN under variable load," *Proceedings of the CSEE*, vol. 37, no. 23, pp. 6943–6950, 2017.

[20] Y. Pan, A. H. Chen, K. F. He, and F. Li, "Rolling bearing diagnosis based on the PF energy characteristics and optimization of neural network," *Journal of Vibration, Measurement & Diagnosis*, vol. 33, no. S1, pp. 120–124, 2013.

[21] L. P. Yan, X. Z. Dongi, Y. J. Zhang, T. Wang, G. Qing, and C. Q. S. Tan, "A gas path fault diagnostic method of gas turbine based on deep belief network," *Journal of Engineering and Thermophysics*, vol. 41, no. 4, pp. 840–844, 2020.

[22] H. Tao, J. Li, Y. Chen, and V. Stojanovic, "Robust point-to-point iterative learning control with trial-varying initial conditions," *IET Control Theory & Applications*, vol. 14, no. 19, 2020.

[23] L. Zhou, H. Tao, W. Paszke, V. Stojanovic, and H. Yang, "PD-type iterative learning control for uncertain spatially interconnected systems," *Mathematics*, vol. 8, no. 9, p. 1528, 2020.

[24] Y. B. Kong, Y. Guo, and X. Wu, "Double-impulse feature extraction of faulty hybrid ceramic ball bearings based on EEMD," *Journal of Vibration and Shock*, vol. 35, no. 1, pp. 17–22, 2016.

[25] J. Z. Xia, L. Zhao, Y. C. Bai, and M. Yu, "Fault feature extraction of rolling element bearings based on Teager energy operator and ZFFT," *Journal of Vibration and Shock*, vol. 36, no. 11, pp. 106–110, 2017.

[26] J. Z. Xia, Y. H. Liu, S. M. Li, Y. G. Leng, and T. Su, "Gearbox fault detection using Hilbert transform and ZFFT," *Journal of Vibration and Shock*, vol. 32, no. 6, pp. 63–66, 2013.

[27] H. Tao, P. Wang, and Y. Chen, "An unsupervised fault diagnosis method for rolling bearing using STFT and generative neural networks," *Journal of the Franklin Institute*, vol. 357, no. 11, 2020.